International Journal of Architectural, Civil and Construction Sciences
ISSN: 2415-1734
Vol:15, No:8, 2021

Influence of Inhomogeneous Wind Fields on the Aerostatic Stability of a Cable-Stayed Pedestrian Bridge without Backstays: Experiments and Numerical Simulations

Yanru Wu, Qing Sun

***Abstract*—**Sightseeing glass bridges located in steep valley area are being built on a large scale owing to the development of tourism. Consequently, their aerostatic stability is seriously affected by the wind field characteristics created by strong wind and special terrain, such as wind speed and wind attack angle. For instance, a cable-stayed pedestrian bridge without backstays comprised of a 60-m cantilever girder and the glass bridge deck is located in an abrupt valley, acting as a viewing platform. The bridge's nonlinear aerostatic stability was analyzed by the segmental model test and numerical simulation in this paper. Based on aerostatic coefficients of the main girder measured in wind tunnel tests, nonlinear influences caused by the structure and aerostatic load, inhomogeneous distribution of torsion angle along the bridge axis, and the influence of initial attack angle were analyzed by using the incremental double iteration method. The results show that the aerostatic response varying with speed shows an obvious nonlinearity, and the aerostatic instability mode is of the characteristic of space deformation of bending-twisting coupling mode. The vertical and torsional deformation of the main girder is larger than its lateral deformation, with the wind speed approaching the critical wind speed. The flow of negative attack angle will reduce the bridges' critical stability wind speed, but the influence of the negative attack angle on the aerostatic stability is more significant than that of the positive attack angle. The critical wind speeds of torsional divergence and lateral buckling are both larger than 200 m/s; namely, the bridge will not occur aerostatic instability under the action of various wind attack angles.

***Keywords*—**Aerostatic nonlinearity, cable-stayed pedestrian bridge, numerical simulation, nonlinear aerostatic stability.

I. Introduction

IN order to enrich sightseeing experience, a cable-stayed pedestrian bridge without backstays consists of a 60-m cantilever girder and glass bridge deck is built on the top of the waterfall. This bridge is located in the area of steep canyon, hence, experiencing stronger gusty wind with higher turbulence intensity, resulting in aerostatic instability. However, the previous researches mainly report the nonlinear aerostatic stability of long-span suspension bridges and cable-stayed bridges with cables on both sides [1]-[4], and most wind codes [5], [6] also do not provide the critical wind speed for the aerostatic instability for such special pedestrian bridges. Therefore, this paper investigates the aerostatic stability of the cable-stayed pedestrian bridge without backstays in the canyon area by numerical simulation.

Generally, the aerostatic deformation of the bridge's main girder will occur under wind load, and then the bridge structure stiffness and the wind load will be altered, as well as increasing the main girder's deformation. Consequently, the bridge's aerostatic instability will occur at a certain critical wind speed. Zhang and Zhou studied the effects of aerodynamic parameters and nonlinear characteristics on suspension bridges [2], [3]. It is worth noting that the critical wind speed of aerostatic stability of long-span bridges may be lower than that of flutter instability based on the wind tunnel test results [4]. Additionally, the nonlinear influences caused by the structure and aerostatic load of long-span bridges cannot be ignored under strong static wind load. The wind speed and wind attack angle along the main girder displayed an inhomogeneous distribution because of the influence of complex terrain in the area of abrupt valley, which also affect the bridge's aerostatic stability [7]. Zhang and Hu analyzed the whole process of aerostatic instability for long-span suspension bridges and cable-stayed bridges, and investigated the effects of three-component coefficients, initial wind attack angle, and wind load on cables and side span on aerostatic stability of long-span cable-supported bridges [8], [9].

The nonlinear aerostatic stability of the bridge was analyzed numerically with considering the influence of inhomogeneous wind field in the abrupt valley. Based on aerostatic coefficients of the main girder measured in wind tunnel tests, the effects of inhomogeneous wind attack angles and inhomogeneous wind speeds on the bridge's aerostatic stability were comprehensively investigated. The aerostatic response of the bridge's main girder was also analyzed.

II. Description and Finite-Element Model of Bridge

A. Description of Bridge

A cable-stayed bridge without backstays comprises a cantilever girder, reinforced concrete arch towers, and glass deck. A lower arch tower embedded in the mountain is inclined at 45°, and the other one embedded in the mountain with pile and anchor is designed with 30° inclination angle. Seven stay

Yanru Wu and Qing Sun are with Department of Civil Engineering, Xi'an Jiaotong University, Xi'an 710049, China (e-mail: wyr4118022017@stu.xjtu.edu.cn, sunq@mail.xjtu.edu.cn).

cables, made of steel, are mounted on each side, and the stay cables fixed on the arch tower have 3.1 m horizontal spacing, while those connected to the main girder are set to have 5.2 m horizontal spacing, as displayed in Fig. 1 (a). The main girders are made of a steel pipe with 110 cm diameter, as illustrated in Fig. 1 (c), and the supporting system adopts the cantilever structure system comprising an arch, girder, and consolidation foundation. The bridge located in the area of abrupt valley would suffer from stronger gusty wind due to the impact of sophisticated terrain, hence, the bridge is prone to aerostatic instability.

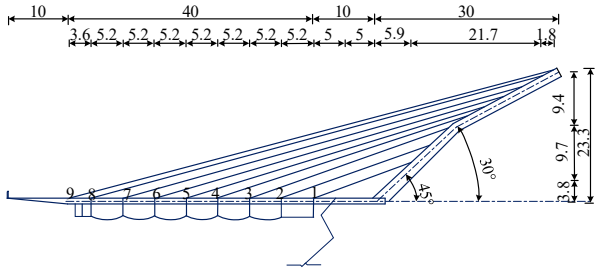

(a) Elevation view of bridge of cables, arch towers, and main girder (units: mm and °)

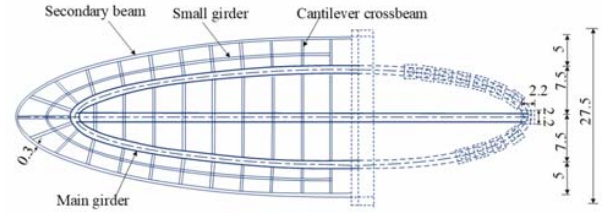

(b) Plan view of the bridge (units: m)

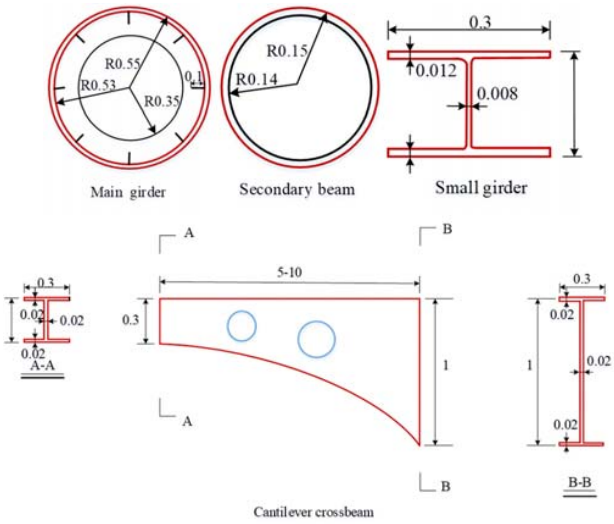

(c) Component sections (units: m)

Fig. 1 Elevation, plan, and components view of bridge

B. Finite-Element Model of Full Bridge

The finite-element model of the bridge is developed by the commercial software ANSYS to investigate the wind characteristics and aerodynamic parameters, as illustrated in Fig. 2. The main girder and pylon are both simulated by the element BEAM 188, and the seven steel stay cables are simulated by the element LINK10. The stay cable-equivalent Young's modulus of elasticity is used to approximate the sagging occurrence in the cables, because it is modelled as truss elements, and the modified elasticity modulus is expressed in (1) [10]:

$$E_r = \frac{E_0}{1 + E_0 \dfrac{(\rho_c g l \cos\alpha_c)^2}{12\sigma^2}} \tag{1}$$

where E_r is the elasticity modulus of the stay cable after considering the sagging effect, E_0 is its original elasticity modulus, ρ_c represents its density, l is its length, α_c is its inclination angle, σ is its average stress, and g is the gravity acceleration.

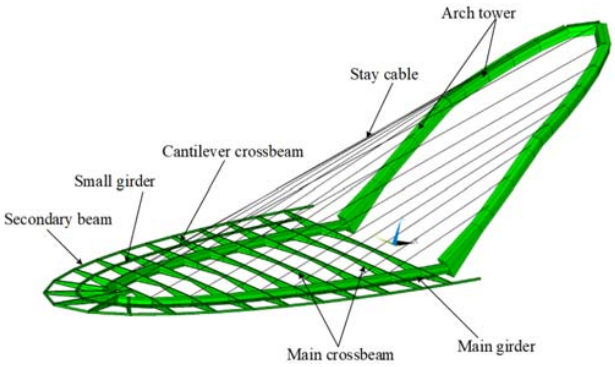

Fig. 2 Finite-element model of the bridge

TABLE I
MODAL PARAMETERS OF THE BRIDGE

Number	Computed prototype frequencies (Hz)	Modal mass (ton)	Mode
1	0.366	79.401	V-1
2	0.614	127.504	L-1
3	0.921	14631.217	T-1
4	1.180	109.869	V-2
5	2.531	1685.015	T-2
6	2.736	89.475	L-2
7	2.878	131.278	V-3
8	4.478	4909.374	T-3
9	4.892	208.908	L-3
10	5.095	282.885	S-B

Note: V, L, and T, respectively, represent the vertical, lateral, and torsional bending of the deck; number represents the mode order; S-B represents the symmetric bending on both sides of main girder.

A geometric nonlinear static analysis is conducted to obtain the structural dynamic characteristics before the modal analysis. The effect of internal force of the structure induced by the dead load is also considered based on the static analysis result. The frequencies of the first symmetric and asymmetric vertical, lateral, and torsional modes are listed in Table I. The

first three mode shapes are vertical, lateral, and torsion, and their corresponding natural frequencies are 0.366, 0.614, and 0.921 Hz (Table I). Obviously, there is a coupling effect between the models because of the longer cantilever main girder.

III. Theory of Static Wind Stability Analysis

A. Static Action of Wind

The average wind load will cause a certain structure deformation in wind field, and the wind load is usually equivalent to a static load [1]-[3]. The load along the main girder's section is decomposed into drag force, lift force, and moment in the wind axis coordinate system, respectively, as shown in Fig. 3. The aerostatic loads per unit span acting on the bridge's main girder can be expressed as functions of transverse wind speed, three-component coefficients, and wind attack angle in the wind axis coordinate system, as expressed in (2)-(4) [7].

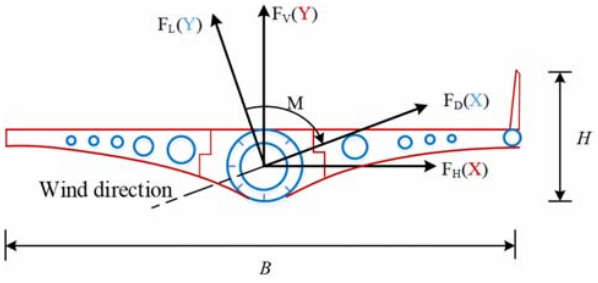

Fig. 3 Definition of wind load in different coordinate system (unit: m)

$$F_D = \frac{1}{2}\rho U^2 C_D(\alpha) H \tag{2}$$

$$F_L = \frac{1}{2}\rho U^2 C_L(\alpha) B \tag{3}$$

$$F_M = \frac{1}{2}\rho U^2 C_M(\alpha) B^2 \tag{4}$$

where F_D, F_L, and F_M are respectively drag force, lift force, and moment in the wind axis coordinate system; B is the width of the girder, $B = 5$ m; H is the whole height of main girder and railing, $H = 2.05$ m, as illustrated in Fig. 3; C_D, C_L, and C_M are the coefficient of drag force, lift force, and moment of main girder, respectively.

The three-component coefficients of the bridge's main girder were measured by the sectional model wind-tunnel tests, in which the scale of the model was 1:50. The sectional model is fixed vertically to the two high-frequency balances installed at the ends of the upstream and downstream of the main girder, and the size of each segment model is shown in Fig. 4. The full bridge is divided into four sections during the test to obtain more accurate experimental data, and the corresponding four models (MOD1, MOD2, MOD3, and MOD4) are developed by removing each segment to obtain the three-component force coefficients. Additionally, the wind speed in the wind tunnel test is set as 7.02 m/s to avoid the lateral sloshing of the model, and the values of turbulence intensity of the oncoming wind speeds was about 2%; concurrently, an automatically controlled dial is adopted to vary the tested wind attack angle.

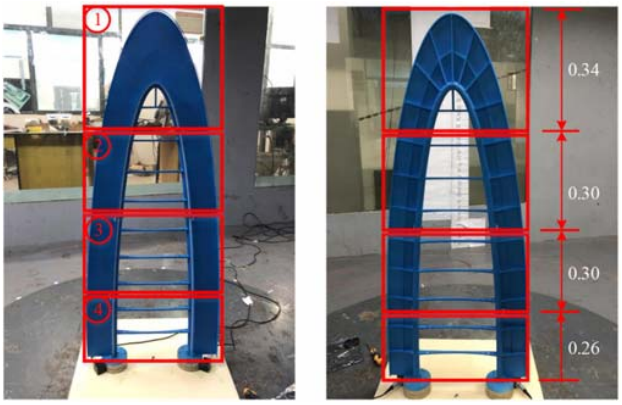

Fig. 4 Sectional model (unit: m)

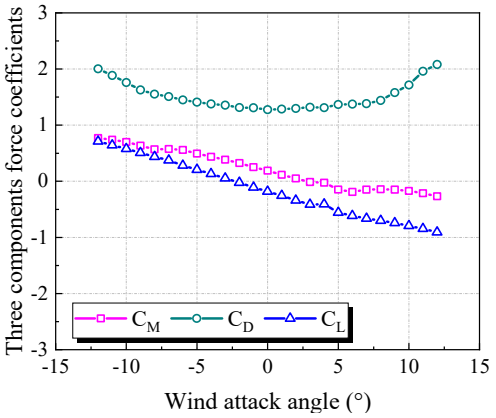

(a) MOD 1

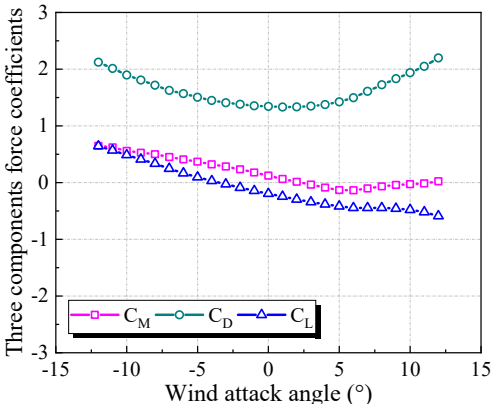

(b) MOD 2

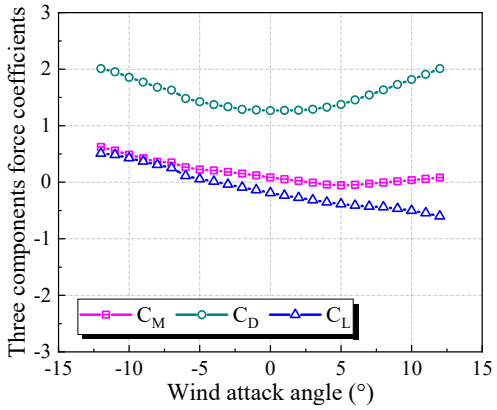

(c) MOD 3

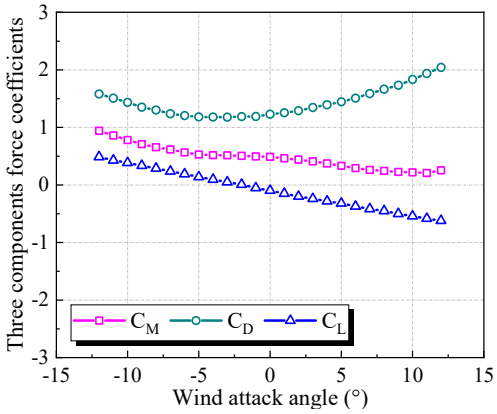

(d) MOD 4

Fig. 5 Three-component force coefficients for the four conditions

Fig. 5 shows that the three-component coefficients of the bridge's main girder change slightly for four models. The coefficients of lift and moment demonstrate negatively correlated relation with wind attack angle. The drag coefficients decrease under the action of negative wind attack angle, but increase under positive attack angle.

B. Analytical Method

Because of the complex cross-section of the pedestrian bridge's main girder, this paper comprehensively considered the nonlinear influences caused by the structure and aerostatic load, and the effect of initial wind attack angle. The incremental double iteration method is used to establish the finite element equilibrium equation, as expressed in (5) [11]:

$$\left[K(\delta)\right]\{\Delta\delta\} = \{\Delta P(\delta)\} \tag{5}$$

where $\left[K(\delta)\right]$ is the structural stiffness matrix; $\{\Delta\delta\}$ is the nodal incremental displacement vector; $\{\Delta P(\delta)\}$ is the nodal incremental wind-loads vector.

Based on the preceding analysis, the aerostatic stability of the cable-stayed pedestrian bridge without backstays can be developed by the ANSYS parametric finite-element analysis method. The specific calculation steps are as follows:

(1) Calculate the three-component forces of each node on the main girder based on the three-component coefficients in Fig. 5.

(2) Determine the initial attack angle on the main girder, $\{\theta\}_0 = \{\theta_1 \quad \theta_2 \quad \cdots \quad \theta_n\}^T = \{\theta_0 \quad \theta_0 \quad \cdots \quad \theta_0\}^T$, and determine the incremental torsion angle vector $\{\Delta\theta\}_0 = \{\Delta\theta_1 \quad \Delta\theta_2 \quad \cdots\cdots \quad \Delta\theta_n\}^T = \{0 \quad 0 \quad \cdots\cdots \quad 0\}^T$.

(3) Use the Newton-Rapson method to obtain the convergence solutions of displacements of the bridge's main girder.

(4) Extract the torsion angle vector of each node on the main girder $\{\theta\}_i = \{\theta_{1i} \quad \theta_{2i} \quad \cdots \quad \theta_{ni}\}^T$, and calculate the incremental torsion angle vector from the differences between the torsion angle vectors of current stage and the previous stage $\{\Delta\theta\}_1 = \{\Delta\theta_{11} \quad \Delta\theta_{21} \quad \cdots\cdots \quad \Delta\theta_{n1}\}^T$, $\Delta\theta_{mi} = \theta_{mi} - \theta_{m(i-1)} - \psi\Delta\theta_{m(i-1)}$, $m = 1,...,n$, and Ψ is the relaxation factor, which equals to 0.4 in this study.

(5) Check if the incremental torsion angle of the main girder is less than the prescribed tolerance, which is taken as 0.005 in this study.

(6) If Step 5 is not satisfied, repeat Steps 2-5 according to the new torsion angle vector for correcting the three-component coefficients, of which the new torsion angle vector $\{\theta\}_n = \{\theta\}_n + \Psi\{\Delta\theta_n\}$.

(7) If Step 5 is satisfied, this means the solutions of current wind speed converges. Then, add the wind speed to calculate the displacements of the bridge's main girder in the next stage

IV. Results and Discussion

The three-component forces of the bridge's main girder and the drag force of stay cables were considered in the numerical analysis. The drag force, lift force, and moment of main girder were calculated by the three-component coefficients measured in wind tunnel tests, and the drag force coefficient was taken as 0.8 specified in the code [6] due to the circular section of stay cables. The three-component forces in the wind axis coordinate system were converted to the drag force, lift force, and moment in the body coordinate system according to the wind attack angle. Additionally, inhomogeneous distribution of wind speed along the bridge's axis is also considered due to the bridge's particularity, and the three-component coefficients obtained by the four sections during the test was adopted.

In order to determine the critical wind speed of the aerostatic instability under homogeneous wind attack angles, the critical wind speed of the aerostatic instability was calculated with initial wind attack angles of -3°, 0°, and +3° according to the preceding analysis method. The evolution between the displacement of mid-span at the main girder's cantilever end and wind speed at three wind attack angles is shown in Fig. 6. The aerostatic responses in three directions at the mid-span of main girder monotonically increase with the increase of wind speed. Obviously, the influence of the negative attack angle on the aerostatic stability is more significant than that of the

positive attack angle. It can be seen from Fig. 6 that when the wind speed is 200 m/s, the vertical displacement, lateral displacement, and torsion angle under the homogenous wind attack angle of -3° changed extraordinarily. However, the aerostatic responses in three directions changed extraordinarily under the homogenous wind attack angle of 0° and +3° as the wind speed is 205 m/s, indicating that the critical wind speed of aerostatic instability under negative attack angle is smaller than that under the positive attack angle. The torsional divergence and lateral buckling critical wind speed are higher than 200 m/s, and much larger than the bridge benchmark wind speed of 116.8 m/s at twice the bridge deck's height according to the JTG/T 3360-01-2018 code [6]. It is indicated that the cable-stayed bridge without backstays will not occur aerostatic instability in the inhomogeneous wind field and homogeneous wind attack angles.

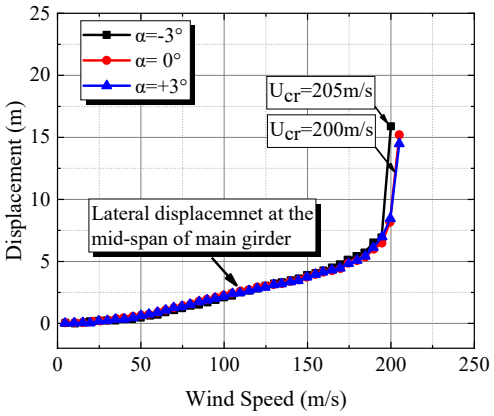

(a)

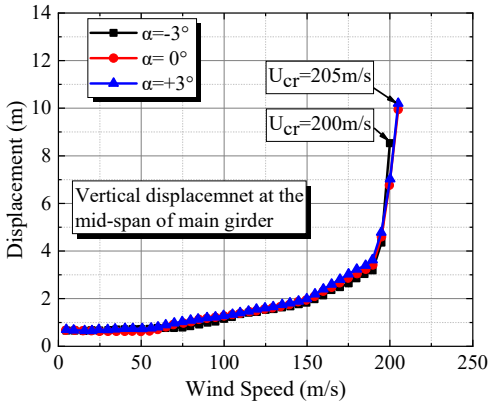

(b)

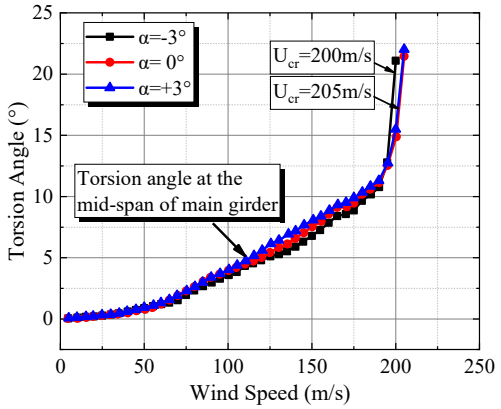

(c)

Fig. 6 Evolution of mid-span girder with wind speed

V. Conclusion

This study focused on the aerostatic stability of a cable-stayed pedestrian bridge without backstays with considering inhomogeneous wind field, as well as considering the influence of initial wind attack angle. The critical wind speed of aerostatic instability under negative attack angle is smaller than that under the positive attack angle, but the influence of the negative attack angle on the aerostatic response is more significant than that of the positive attack angle.

The torsional divergence and lateral buckling critical wind speed are higher than 200 m/s, and much larger than the bridge benchmark wind speed of 116.8 m/s at twice the bridge deck's height. It indicates that the cable-stayed bridge without backstays will not occur aerostatic instability in the inhomogeneous wind field and homogeneous wind attack angles.

Acknowledgment

This study was financially supported by the National Natural Science Foundation of China (Grant No. 51978570), which is gratefully acknowledged.

References

[1] M. Xu, W. W. Guo, H. Xia, et al. Nonlinear aerostatic stability analysis of Hutong cable-stayed rail-cum-road bridge. J. Wind and Structures, 2016, 23(6): 485-503.
[2] W. M. Zhang, K. R. Qian, L. Wang, et al. Aerostatic instability mode analysis of three-tower suspension bridges via strain energy and dynamic characteristics. J. Wind and Structures, 2019, 3(29):163-175.
[3] Q. Zhou, H. L. Liao, T. Wang. Numerical study on aerostatic instability modes of the double-main-span suspensions bridges. J. Shock and Vibration, 2018(PT.1): 7458521-7458529.
[4] F. H. Dong, J. Cheng. A new method for estimation of aerostatic stability safety factors of cable-stayed bridges. J. Proceedings of the Institution of Civil Engineers-Structures and Buildings, 2019, 172(1): 17-29.
[5] American society of civil engineers. ASCE/SEI 7-10, New York, 2010.
[6] Wind-resistent Design Specification for Highway Bridges. JTG/T 3360-01-2018, China. (In Chinese)
[7] P. Hu, Y. Han, G. Xu, et al. "Numerical simulation of wind fields at the bridge site in mountain-gorge terrain considering an updated curved boundary transition section." J. Aerosp. Eng. 2018, 31 (3): 04018008.
[8] Z. T. Zhang, Y. J. Ge, and Z. Q. Chen. "On the aerostatic divergence of suspension bridges: A cable-length-based criterion for the stiffness

degradation." J. Fluids Struct. 2015, 52 (Jan): 118–129.
[9] P. Hu, Y. Han, G. J. Xu, et al. Effects of inhomogeneous wind fields on the aerostatic stability of a long-span cable-stayed bridge located in a mountain-gorge terrain. J. Journal of Aerospace Engineering, 2020, 33(3):04020006.
[10] J. Y. Zhang, M. J. Zhang, Y. L. Li, et al. Comparison of wind characteristics at different heights of deep-cut canyon based on field measurement. Advances in Struct. Engi. 2020, 23(2), 219-233.
[11] Z. Q. Chen, Bridge Wind Engineering. China Communications Press. China, Beijing, 2005. (In Chinese)